Published April 22, 2016

Topographic and Geologic Controls on Soil Variability in California's Sierra Nevada Foothill Region

D.E. Beaudette*
USDA-NRCS - Soil Survey
19777 Greenley Rd
Sonora, CA 95370

A.T. O'Geen
University of California Davis
Land, Air and Water Resources
One Shields Ave
Davis, CA 95616

We evaluated the feasibility of quantitative soil mapping in two catenas established on different lithologies (metavolcanic and granitic) in the Sierra Foothill Region of California. Indices of landform and microclimate were extracted from a 1-m elevation model. Variation in soil "character" (clay content, pH, color, cation-exchange capacity [CEC], and Fe_o/Fe_d) was partitioned across variables associated with terrain shape and microclimate, lithologic variability, and sampling depth. The potential for using digital elevation models (DEM)-derived indices of terrain shape to predict spatial patterns in soil properties varied greatly between our two experimental catenas. Terrain shape accounted for 4% (metavolcanic site) to 30% (granitic site) of variance in soil properties, while lithology accounted for 14% (metavolcanic site) to 22% (granitic site) of variance in soil properties. Sample depth accounted for 3% (metavolcanic site) to 12% (granitic site) of variance in soil properties. At the metavolcanic site, variability in lithology contributed more to soil variation than terrain shape, which makes digital soil modeling efforts a challenge in these regions. Up to 66% of the variance in soil properties was explained at the granitic site when considering terrain, lithology, sample depth, and associated interactions of these variables. Variance proportions can provide insight into the relative importance of soil-forming factors and is a useful tool when evaluating the efficacy of digital soil mapping projects.

Abbreviations: CEC, cation-exchange capacity; CS, conditional simulation; CTI, compound topographic index; DEM, digital elevation models; OK, ordinary kriging; pRDA, partial redundancy analysis; PCA, principal components analysis; QSM, quantitative soil mapping; RDA, redundancy analysis; RCS, restricted cubic splines; RST, regularized splines in tension; RTK, real-time kinematice; SFR, Sierra Nevada Foothill Region; SFREC, Sierra Foothill Research and Extension Center; SJER, San Joaquin Experimental Station; TCI, terrain characterization index; XRF, x-ray fluorescence.

Core Ideas

- **Lithologic variability is often greater than expected.**
- **Variance partitioning methods can untangle superposed soil-forming processes.**
- **RDA is a convenient framework for interpreting complex soil-landscape relationships.**

The development and application of the soil–landscape paradigm has played a significant role in how soil scientists conduct research, interpret and communicate their findings, and apply the resulting knowledge to solve real-world problems (Hudson, 1992). Within this framework, repeating patterns in soil properties or classes are correlated with factors that drive redistribution of sediment (slope angle), effective precipitation (surface curvature), and microclimate (slope aspect); and are stratified according to differences in parent material, biota, and time. Traditionally, this approach has been implemented through qualitative evaluation (i.e., mental models) of Hans Jenny's (Jenny, 1941) state-factor model of soil genesis. Modern extensions to this framework for mapping soils commonly termed digital soil mapping are based on a numerical integration of soil property or class data with quantitative proxies of soil-forming factors (Moore et al., 1991; Scull et al., 2003; Brown et al., 2004; Grunwald, 2009). In an era where nearly all scientific work is performed "digitally", the authors of this

Soil Sci. Soc. Am. J. 80:341–354
doi:10.2136/sssaj2015.07.0251
Supplemental material is available online.
Received 2 July 2015.
Accepted 4 Jan. 2016.
*Corresponding author (debeaudette@ucdavis.edu).

study chose an alternative label, quantitative soil mapping, for the suite of techniques commonly described as "digital soil mapping" (McBratney et al., 2003). After all, these techniques are extensions to the basic concepts Jenny presented as "a system of quantitative pedology", enabled by recent advances in analytical and computational resources.

Some of the approaches commonly used for quantitative soil mapping (QSM) include: 1. Statistical models linking soil properties to environmental and terrain parameters (regression; McKenzie and Ryan, 1999; Gessler et al., 2000; Thompson et al., 2006; Indorante et al., 2014); 2. interpolation based on a model of spatial structure (geostatistics; Goovaerts, 1999); and, 3. multivariate techniques such as cluster analysis, discriminant analysis, or dimension reduction strategies (principal component analysis [PCA], multidimensional scaling, or ordination techniques; Verheyen et al., 2001; Young and Hammer, 2000; Hengl and Rossiter, 2003; Odeh et al., 1991). It is also possible to integrate elements of these different approaches into hybrid techniques such as regression kriging (Hengl et al., 2004), interpolation of taxonomic distances (Carre and McBratney, 2005), or supervised classification constrained by taxonomic distance (Minasny and McBratney, 2007). An observed lack of consistency among QSM approaches in the published literature (Grunwald, 2009) suggests that certain landscapes are more amenable to QSM than others.

Quantifiable relationships between soil properties and soil forming factors are often complicated by the vertical anisotropy within soil profiles. Models based on soil properties sampled by genetic horizons must further account for variable horizon depths. Various parametric (Myers et al., 2011) and spline functions (Bishop et al., 1999; McBratney et al., 2000; Malone et al., 2009) have been used to accommodate vertical anisotropy and variable horizon thickness. An alternative approach based on the evaluation of percentiles along 1-cm depth slices, or larger "slabs" (e.g., 10-cm sections), was suggested by Beaudette et al. (2013b). Explicitly accounting for these complexities has the potential to create a more robust model that incorporates three-dimensional soil property data.

The development, application, and predictive capacity of QSM methods ultimately depends on the relative intensity of individual soil forming factors and the degree to which adequate proxies for these factors can be identified. Our goal was to evaluate the predictive capacity for QSM in the Sierra Nevada Foothill Region (SFR), within two contrasting landscapes underlain by granite in the south (San Joaquin Experimental Station [SJER]) and metavolcanic rocks in the north (Sierra Foothill Research and Extension Center [SFREC]). We were interested in determining the strength of relationships between measured soil properties and several terrain-based proxies for microclimate and redistribution processes (e.g., sediment and water), in the presence of complex lithologic variability, using a "variance partitioning" framework. Covariates describing vertical anisotropy were included in the variance partitioning framework for two reasons: (i) as a benchmark to compare against, for example, does topography contribute to more variation than processes occurring within the soil profile? and, (ii) as a covariate to support spatial analysis of three-dimensional data. We hypothesized that terrain-based proxies for near surface processes would account for a larger proportion of (horizon-scale) soil property variability than variability with depth. In addition, we hypothesized that QSM techniques would perform better in the weakly developed (less vertical anisotropy) soils of the rolling granitic landscapes as compared with the well-developed (more vertical anisotropy) soils in metavolcanic landscapes because of the complex feedback mechanisms associated with lateral water movement, perched water tables, and pedogenic processes in well-developed soils (Swarowsky et al., 2012).

MATERIALS AND METHODS

Soils were sampled from two representative lithologies from the SFR, granitoid rocks in the south at the SJER, and metavolcanic rocks in the north at the SFREC. Details about the environmental settings of these sites are described in previous work (Swarowsky et al., 2012; Beaudette et al., 2013a).

A 30-ha collection of interconnected catenas was selected to represent the rolling terrain at SJER. Here, local geology is dominated by Mesozoic granodiorite with patches of granite, tonalite, and diorite. Soils at SJER are typical of those mapped within this region: Ahwahnee (coarse-loamy, mixed, active, thermic Mollic Haploxeralfs) on summit positions, and Vista (coarse-loamy, mixed, superactive, thermic Typic Haploxerepts) on the backslope positions (Soil Survey Staff, 1999). Elevation within the SJER catena extends from 330 to 370 m, mean annual precipitation (MAP) is 500 mm, and mean annual average temperature (MAAT) is 16.0°C.

A single 30-ha headwater catchment was selected to represent the steep, complex sequence of landforms at SFREC. Here the geology is dominated by Mesozoic metavolcanic rocks (greenstone) of the Smartville complex. Dominant soils included: Sobrante (Fine-loamy, mixed, active, thermic Mollic Haploxeralfs) and Timbuctoo (Fine, parasesquic, thermic Typic Rhodoxeralfs), both occurring on backslope and summit positions. Elevation within the SFREC catena extends from 160 to 410 m, MAP is 705 mm, and MAAT is 16.6°C.

Soil Profile Sampling and Laboratory Characterization

Sampling locations were selected according to a random-stratified design (de Gruijter et al., 2006) within expert-delineated landscape positions. At each location, morphological characteristics were described, and soil samples were collected by genetic horizon for laboratory analysis. A total of 15 soil profiles from SJER were described and sampled, with an additional 26 supplemental auger observations where abbreviated descriptions of morphology, soil depth, and paralithic materials were recorded (Fig. 1). A total of 106 soil profiles from SFREC were described (Soil Survey Staff, 2012) and sampled, with laboratory characterization performed on approximately two-thirds of the profiles (Fig. 1). All analyses (except elemental analysis) were performed on air-dried soil mate-

rial that had been gently crushed and passed through a 2-mm sieve. A subset of this soil material was powdered and homogenized in a ball mill for 24 h. Ball-milled soil samples were packed into sample cups and sealed with polypropylene film (Premier Lab Supply) for elemental analysis.

Laboratory characterization of the <2-mm fraction included particle-size analysis [pipette method (Gee and Orr, 2002)], CEC [$NH_4OCH_3O_2H$ at pH 7 (Soil Survey Staff, 2004)], selective dissolution of Fe and Mn [citrate–bicarbonate–dithionite and acid-oxalate (McKeague and Day, 1966)], pH [1:1 soil/water (Soil Survey Staff, 2004)], and total carbon (combustion-gas chromatography).

Elemental analysis was performed using two portable X-ray fluorescence (XRF) devices within a shielded enclosure and controlled sample presentation system. A 3 min run-time on the Thermo-Fisher XL3T-800 in "soil mode" was used to measure elements with expected concentrations <1%, and a 3 min run-time on the Thermo-Fisher XL3T-900 GOLDD in "mining mode" was used to measure elements with expected concentrations >1%. The use of polypropylene film and combination of detection modes was suggested by a Thermo-Fisher application scientist to maximize detection accuracy of elements lighter than Ti (Laura Stupi, personal communication, 2010).

Total soil Fe, Ca, and Zr (measured by XRF) were used as indices of lithologic variability within both catenas. Total Ca and Fe were used to describe gradation from granodiorite (lower occurrence of Ca and Fe-bearing minerals) to diorite (higher relative occurrence of Ca and Fe-bearing minerals) at SJER, and gradation from intermediate (high Ca, moderate Fe) to mafic (low Ca, high Fe) rocks at SFREC. Zirconium was included in this suite of indicator elements because minerals that contain Zr in the soil are typically resistant to weathering and translocation processes, and therefore useful indicators of parent material provenance (Fitzpatrick and Chittleborough, 2002).

Soil color was measured using a Konica-Minolta CR-410 colorimeter (Liles et al., 2013). The CIELAB colorspace was used (Viscarra Rossel et al., 2006). The positive A-axis was used to represent soil sample redness.

Iron and Mn crystallinity indices were computed as the ratio of acid-oxalate extracted element to citrate–bicarbonate–dithionite extracted element. An iron oxide accumulation index was computed as the ratio of citrate–bicarbonate–dithionite extracted Fe to total Fe content as measured by XRF (Fe_d/Fe_{total}). This index was used to describe soil development in the presence of lithologic variability.

Rock samples were collected from outcroppings in each catena; 2 sites at SJER, and 10 sites at SFREC (Fig. 1). Rock samples were crushed and digested in concentrated acid (HNO_3–$HClO_4$–HF- HCL). Total elemental analysis was performed via inductively coupled plasma emission spectrometry (ICP-ES).

Characterization of Lithologic Variability

Interpolated maps of horizon thickness-weighted mean Fe (total soil Fe as measured by XRF) were generated for each catena, using conditional simulation at SJER and ordinary kriging at SFREC (Issaks and Srivastava, 1989). Spatial auto-correlation was parameterized using a spherical variogram model within each catena, having: partial sills of 2.8 Fe $\%^2$ (SJER) and 4.1Fe$\%^2$ (SFREC), ranges of 100 m (SJER) and 650 m (SFREC), and nugget variances of 0.1Fe $\%^2$ (SJER) and 0.2Fe $\%^2$ (SFREC). Conditional simulation (CS) was used in favor of ordinary kriging (OK) due to the small number of sampling locations at SJER. Total soil Fe values at SJER were computed by taking the pixel-wise mean of 100 conditional simulations. These values were converted into classes using a set of rules based on mean Fe-

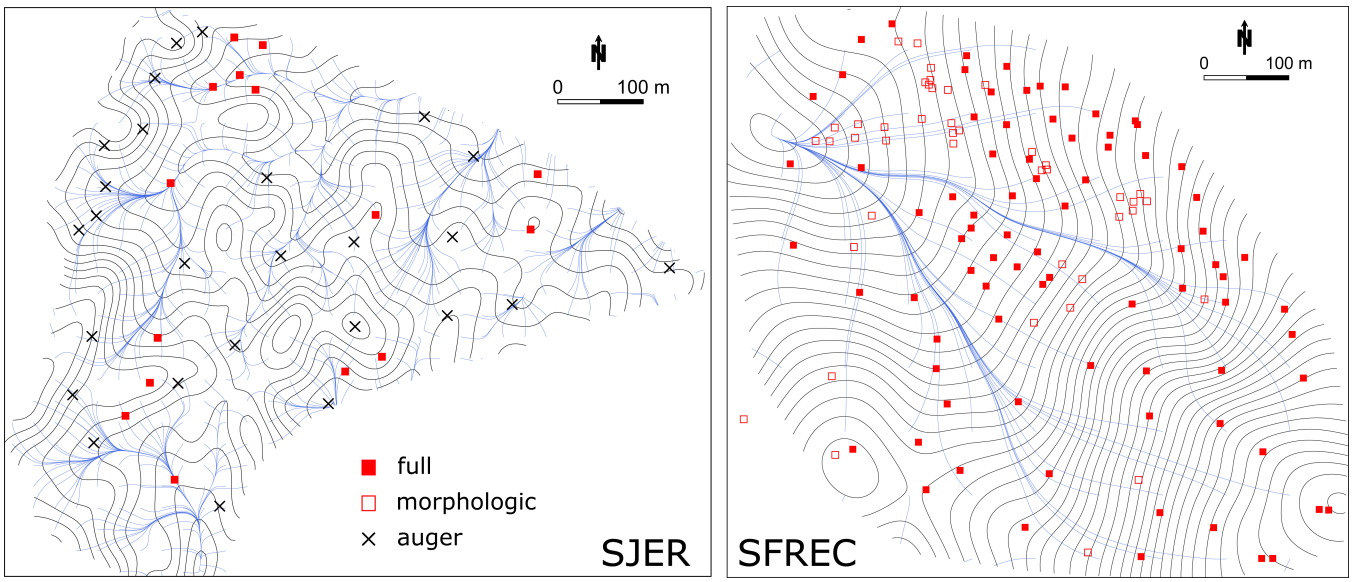

Fig. 1. Sampling locations (point symbols), elevation contours (solid black lines—2-m interval at SJER, 5-m interval at SFREC), and estimated paths of flow-line convergence (solid blue lines) within each catena. Filled symbols represent locations where laboratory characterization was performed on soil samples, open symbols represent points where only morphological data were collected. Black 'x' symbols (San Joaquin Experimental Station, SJER) represent auger sampling locations.

contents of granite, granodiorite, and diorite (Le Maitre, 1976): "granite" (1% < Fe $\leq$ 2.5%), "granodiorite" (2.5% < Fe $\leq$ 4.5%), and "diorite" (4.5% < Fe). Principal component analysis was used to investigate the relationship between total soil Fe, Ca, and Zr concentrations within each catena.

Digital Terrain Modeling

A detailed elevation survey was conducted at both catenas (approximately 1000 measurements each) with a Trimble R7 real-time kinematic (RTK) GPS. Primary topographic parameters (slope angle, aspect angle, profile curvature, tangential curvature, and mean curvature) were generated from partial first and second derivatives of the elevation surface fit by regularized splines in tension (RST) interpolation (Mitasova and Mitas, 1993). Secondary topographic parameters including the compound topographic index (CTI; Wilson and Gallant, 2000), Llobera's topographic prominence index (Llobera, 2001), annual beam radiance (Rigollier et al., 2000), flowline density (Mitasova and Hofierka, 1993; GRASS Development Team, 2009), distance from flowline, upslope contributing area (GRASS Development Team, 2009), and terrain characterization index (TCI; Park et al., 2001) were computed within GRASS GIS (GRASS Development Team, 2009). Details on the topographic survey and calculation of terrain attributes are described in Beaudette et al. (2013a).

Statistical Analysis

Variation in horizon depths, thickness, and the presence or absence of major horizon types makes it difficult to investigate relationships between (horizon scale) soil properties associated with genetic horizons and corresponding (pedon scale) terrain attributes. Two approaches were used to overcome this problem: 1. Horizon-scale soil property data were aggregated to the profile scale using horizon thickness-weighted averages, and 2. Soil property data were aligned to a regular sequence of 10 cm-thick depth "slabs" using thickness-weighted averages when slabs included more than one genetic horizon (Beaudette et al., 2013b).

Characterization of Vertical Anisotropy

We used restricted cubic splines (RCS) to describe collections of soil property depth-functions because these functions require few assumptions (e.g., no smoothing parameters) and are linear in the tails (Harrell, 2001). Four RCS basis functions were generated using a natural spline basis matrix (four degrees of freedom) constrained at three interior knot locations (Hastie et al., 2009). Interior knots at equal depth intervals (37.5, 75.0, and 112.5 cm) were used instead of horizon midpoints, as horizonation varied greatly within and between each catena. Additive combinations of the RCS basis functions can be used within the context of regression and ordination methods to describe smooth, nonlinear soil property depth-functions (Supplemental Figure A). As with any regression model, the use of RCS basis functions requires sufficient sample size to accommodate additional predictor variables. Resampling horizons (e.g., via "slab" approach outlined in *Statistical Analysis* section above) to a common depth-interval ensures that horizon-level properties are equally weighted within a regression model that includes RCS basis functions.

Univariate Soil-Landscape Relationships

The relationships between profile-scale aggregate soil property data and terrain attributes were determined using Spearman's rank correlation coefficient (Verzani, 2004). Tied ranks within either data series were averaged. The Spearman rank correlation coefficient (r_s) ranges from -1 to 1, and is useful for determining the strength of a relationship when nonlinear, but monotonic, patterns are hypothesized.

Multivariate Soil-Landscape Relationships

A more comprehensive evaluation of soil-landscape relationships was based on the magnitude of variance in several soil properties explained by a collection of terrain shape and lithologic indices. We used redundancy analysis (RDA) to investigate multivariate soil-landscape relationships, based on horizon thickness-weighted mean soil properties. Redundancy analysis is an extension of multiple linear regression (single response variable, multiple predictor variables) to systems involving several response variables (Legendre and Legendre, 1998). Analogous to PCA, an RDA solution is an ordination of predictor variables; however, the RDA-based ordination is constrained such that the RDA "scores" are linear combinations of both predictor and response variables.

The RDA "triplot" (Supplemental Figure B) is a standard method used to display results from RDA, where observations are plotted onto a coordinate system defined by two RDA axes. On these new axes, inter-point proximity is approximately proportional to numerical similarity (RDA scaling Type II). Vectors representing predictor and response variables are added to the plot, such that: 1. Angles between (X and Y) variables represent correlation (maximum positive correlation at 0 degrees, maximum negative correlation at 180 degrees, and minimum correlation at 90 or 270 degrees); 2. Right-angle projections of an observation along either response or predictor vectors approximates the value of the variable for that observation. Vector length and direction with respect to RDA axes denote relative contribution to—(in the case of predictor variables) or degree of associated with—(in the case of response variables) RDA axes.

Variance Partitioning

We used partial RDA (pRDA) to evaluate what proportion of variance in a suite of measured soil properties ("soil character") was explained by geographically associated measurements of "terrain character" and "lithologic character" (Legendre and Legendre, 1998). The association between a multivariate response and several predictor variables was modeled as:

$$\left|y_1\ y_2\ y_3\right| \sim x_1 + x_2 + x_3 + x_4 + x_5 + x_6 + x_7 + x_8 + x_9$$

$$\left|y_1\ y_2\ y_3\right| \sim \left|a_1 a_2 a_3\right| + \left|b_1\ b_2\ b_3\right| + \left|c_1 c_2 c_3\right| \qquad [1]$$

$$\mathbf{Y} \sim \mathbf{A} + \mathbf{B} + \mathbf{C}$$

where $|y_1y_2y_3|$ represent a multivariate response, and x_1 though x_9 represent predictor variables. Partial RDA partitions variance in the multivariate response across sets of predictor variables (e.g., $|a_1a_2a_3|$ vs. $|b_1b_2b_3|$ vs. $|c_1c_2c_3|$). Soil properties used to define "soil character" (**Y** from Eq. [1]), included: clay content, CEC, pH, redness, and Fe crystallinity (Fe_o/Fe_d). Terrain attributes used to define "terrain character" (**A** from Eq. [1]) included CTI, annual beam radiance, slope angle, profile curvature, and mean curvature. Elemental concentrations used to define "lithologic variability" (**B** from Eq. [1]) included total soil Ca, Fe, and Zr. Restricted cubic spline basis functions (4) used to describe vertical anisotropy (**C** from Eq. [1]) were also included (Supplemental Figure A, left panel). This analytical framework made it possible to partition variance in "soil character" across terrain metrics, indices of lithologic variability, and depth. All variables were centered (subtraction of mean) and scaled (division by standard deviation) before RDA and pRDA analysis, to accommodate multiple units of measure (Legendre and Legendre, 1998). All statistical analyses were performed with R (R Core Team, 2014) version 3.1.1. RDA and pRDA analyses were performed using the "vegan" package for R (Oksanen et al., 2015).

RESULTS AND DISCUSSION

Soil Morphology and Properties

The residual and colluvial soils formed on granite at SJER were moderately deep (≈80% were ≥75 cm) to deep (≈33% were ≥100 cm). A small fraction were shallow (≈10% were <50 cm). Of the moderately deep or deeper soils at SJER, A horizons most commonly occurred within the upper 15 cm, AB horizons at 15 to 30 cm, Bw or Bt horizons at 30 to 80 cm, and C horizons or the Cr contact were present from 80 to 120+ cm (Fig. 2).

The residual and colluvial soils formed on metavolcanic rock at SFREC varied greatly in depth ranging 20 to over 150 cm, however, most were moderately deep (≈72% ≥ 80 cm) to deep (≈44% ≥ 100 cm), with a small fraction of shallow soils (≈5% < 50 cm; Fig. 2). The larger number of described profiles at SFREC resulted in smoother horizon probability estimates (Fig. 2), with A horizons common in the upper 8 cm, BA horizons at 8 to 20 cm, Bt horizons from 20 to 80+ cm. Contact with Cr material or bedrock was highly variable, but typically near 60 cm (shallower soils) or near 90 cm (deeper soils). Clay-rich horizons, usually > 40% clay by weight, locally referred to as "claypans", were present in some (24%) SFREC soils, from 30 to 100 cm (Fig. 2).

Soils derived from metavolcanic rock at SFREC were finer textured, and had higher CEC, total carbon, redness, and total soil Fe compared with SJER. Soils derived from granite at SJER had slightly higher pH, a greater proportion of poorly crystalline Fe and Mn, and greater total soil Ca, Zr, and Si concentrations (Fig. 3). Strong vertical differentiation at SJER was present in a few measured soil properties: 1. Iron crystallinity generally increased with depth as indicated by a decrease in Fe_o/Fe_d values. 2. Deep soils had higher pH values below 80 to 100 cm. At SFREC, two major vertical trends were apparent: clay content and CEC (Fig. 3). The large increase in clay with depth from 20 to 80 cm coincided with the range of described Bt horizons. Abrupt increase in CEC variability from 60 to 100 cm corresponded to the range of described claypan features, which contained a larger proportion of smectite group minerals compared with overlying horizons. Total carbon content in the top 40 cm was typically 0.25 to 1.5% (absolute) greater at SFREC due to higher precipitation (705 mm at SFREC vs. 500 mm at SJER) and greater overall primary production. Total carbon values

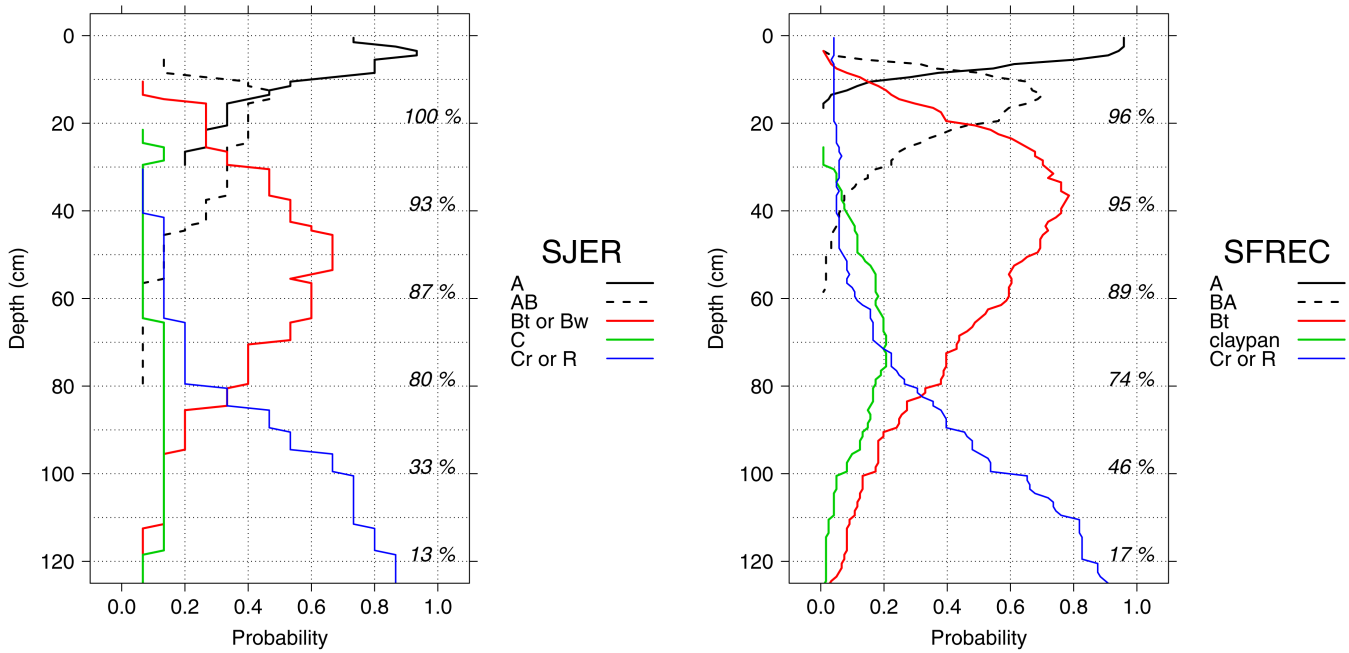

Fig. 2. Probability depth-functions for major horizon types, at the San Joaquin Experimental Range (SJER) and Sierra Foothill Research and Extension Center (SFREC). Percentages printed along the right-hand side of the depth axis describe the percentage of profiles contributing to probability calculations. "Claypan" features at SFREC were described as 2Bt horizons, and generally contained > 40% clay by weight.

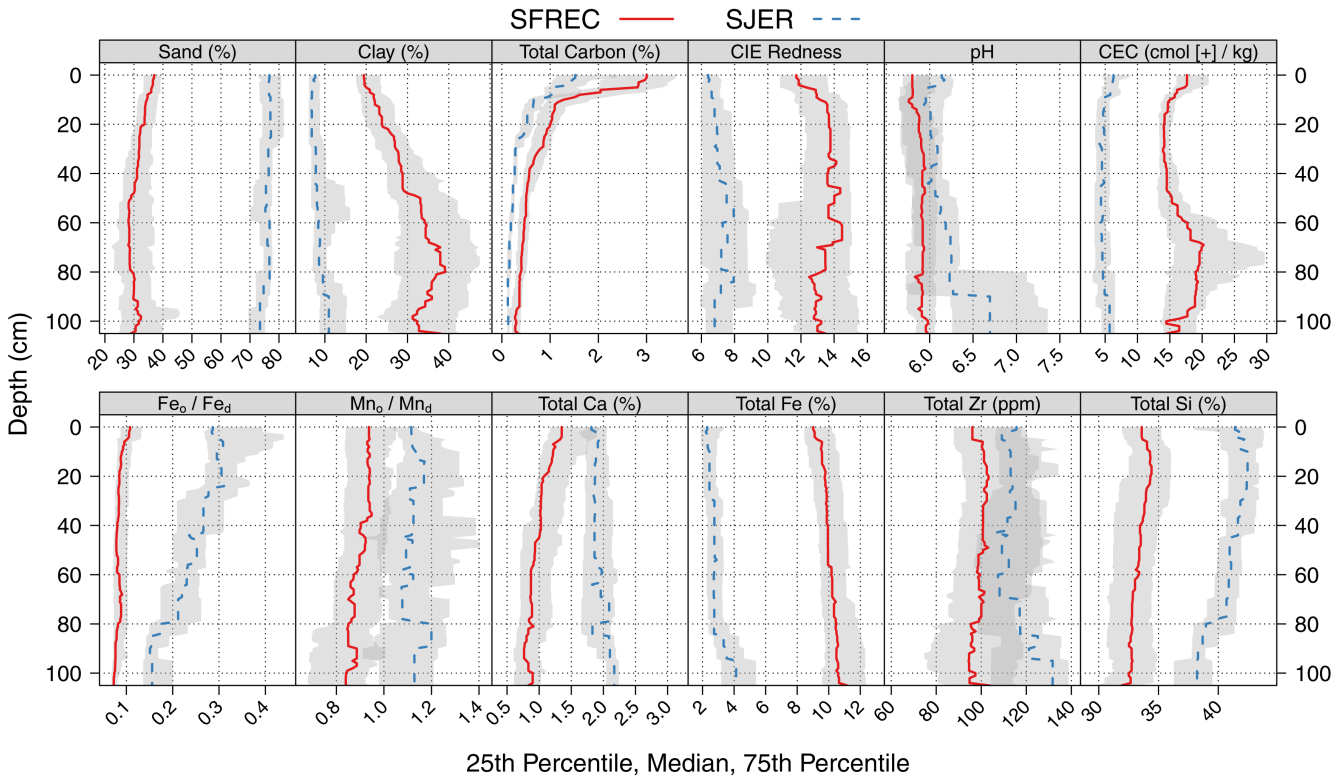

Fig. 3. Soil properties and total elemental concentration depth-functions, grouped by catena. Median values are plotted as lines, bounded by 25th percentile and 75th percentile (gray region). CIE Redness values are positive values from the A-axis of the CIELAB color-space, where larger values correspond to redder hues. Fe and Mn crystallinity values are based on the ratios of Fe_o/Fe_d and Mn_o/Mn_d, respectively. Data were aggregated over 1-cm depth slices.

from 15 to 30 cm (SJER) and from 10 to 40 cm (SFREC) deviated from the typical exponential decay-shaped depth-function (Mishra et al., 2009) and were likely related to the heavily bioturbated AB (SJER) and BA (SFREC) horizons described within these depth intervals.

Table 1. Summary statistics for select terrain attributes, sampled from digital elevation model (DEM)-derived surfaces at soil pit locations. A graphical comparison of mean curvature, annual beam radiance, and compound topographic index (CTI) is presented in Beaudette et al. (2013a).

Site	Statistic	Slope	Tang. curv.†	Profile curv.‡	Mean curv.§	Top. prom.¶	Ann. beam radiance	CTI	TCI
		%	——————m^{-1}——————				–MJ m^2–		
SJER	Min	2	-8.5E-03	-6.8E-03	-4.7E-03	-0.97	59300	4.1	-1.6E-02
	Q25	4	-3.3E-03	-4.0E-03	-3.6E-03	-0.53	66500	4.6	-6.4E-03
	Median	11	-6.9E-05	-8.8E-04	-1.8E-03	-0.09	68800	5.6	-2.4E-03
	Mean	9	-4.3E-04	-4.9E-04	-4.6E-04	-0.08	67800	6.4	-3.8E-03
	Q75	13	4.0E-03	9.6E-04	1.9E-03	0.35	71200	6.6	10E-04
	Max	19	6.6E-03	1.1E-02	7.7E-03	0.98	72100	11.9	5.3E-03
SFREC	Min	5	-8.5E-03	-7.5E-03	-5.2E-03	-0.93	37500	4.4	-1.6E-02
	Q25	21	-8.1E-04	-1.4E-03	-1.1E-03	-0.37	57600	5.7	-2.7E-03
	Median	27	4.2E-04	-3.4E-04	-9.5E-05	-0.08	63500	6.1	-2.1E-04
	Mean	27	2.3E-04	-2.4E-04	-2.9E-06	-0.001	61200	6.3	-6.3E-04
	Q75	32	1.6E-03	6.9E-04	9.1E-04	0.37	65800	6.7	1.8E-03
	Max	61	9.1E-03	5.1E-03	5.8E-03	0.99	71700	10.4	9.0E-03

† Tangential Curvature.

‡ Profile curvature.

§ Mean curvature.

¶ Topographic prominence; CTI-compound topographic index (unitless); TCI-terrain characterization index (unitless).

Terrain Attribute Selection

Terrain attribute summaries illustrate differences between landscapes at each catena (Table 1). Landforms at SFREC were characterized by steeper and longer slope lengths compared with SJER. Range in modeled annual beam radiance was greater at SFREC, due to increased local shading by adjacent terrain units. It was not possible to sample soils with CTI values greater than 10.5 at SFREC as these portions of the landscape had been scoured of all soil material. In contrast, landscape positions at SJER with CTI values as high as 12 were common, and associated with deep soils in swale positions.

With the exception of modeled annual beam radiance, most of the terrain attributes evaluated in this study were moderately to strongly correlated, with a pronounced grouping of attributes related to flow convergence (Fig. 4). Stronger correlation between slope and annual beam radiance at SFREC (r_s = 0.15 vs. r_s = 0.01 at SJER) was likely related to the greater influence of localized shadowing characteristic of the steep terrain. The strong correlation between mean curvature and TCI was not surprising given its

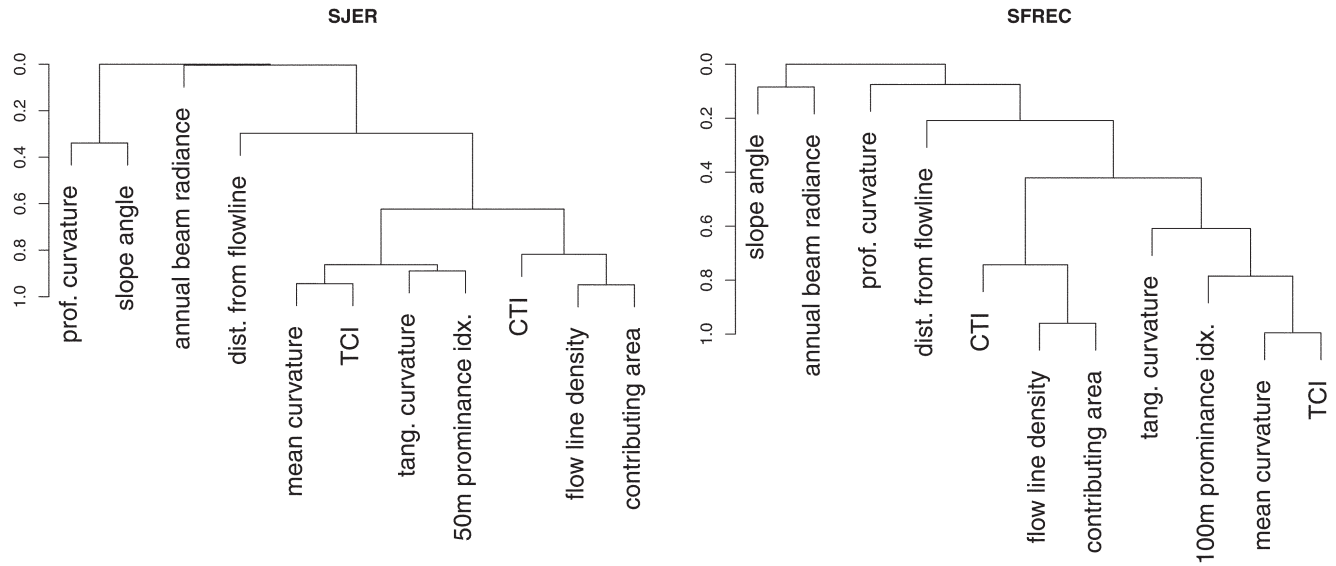

Fig. 4. Terrain variable correlation structure, based on Spearman rank correlation coefficients. Branching level and y-axis labels describe the magnitude of the squared Spearman rank correlation between variables: that is, branching at lower positions in the figure denotes higher correlation within groups of variables.

derivation. However, correlation between CTI and TCI (r_s = 0.65 at SJER and r_s = 0.40 at SFREC) was lower than expected, as both indices estimate flow convergence. The high degree of correlation within the suite of DEM-derived terrain attributes suggests that a subset was sufficient for modeling soil–landscape relationships. Thus, five of the least-correlated terrain attributes were selected to represent major landscape processes: annual beam radiance (microclimate), slope (localized mass-wasting potential), profile curvature (two-dimensional localized shedding vs. collecting), mean curvature (three-dimensional localized shedding vs. collecting), and CTI (catchment-scale focusing of moisture and sediment).

Correlation between Terrain Attributes and Aggregated Soil Properties

Mean curvature and CTI had the largest correlation with soil properties in granitic terrain at SJER, followed by profile curvature, annual beam radiance, and slope angle (Table 2). Statistically significant ($p < 0.05$) Spearman correlation coefficients were limited to the range of about $\{0.5 \leq |r_s| \leq 1.0\}$ due to the small sample size at SJER. At this level of significance, the absolute value of the mean correlation between all pairs of aggregate soil properties and terrain attributes was 0.61. Mean curvature, profile curvature, and CTI accounted for major differences in soil properties as stratified by "upland" (summit and shoulder/lower CTI and positive curvatures) vs. "lowland" (footslope and swale/higher CTI and negative curvatures) positions at SJER. These patterns largely follow what the standard soil-landscape model predicts transport of sediment and weathering products from divergent landscape positions (e.g., shallower soils, lower relative pH, lower relative CEC, more intense reddening) to convergent landscape positions (e.g., deeper soils, higher relative pH, higher relative CEC, presence of redoximorphic features; Table 2; Ruhe, 1956; King et al., 1983). Modeled annual beam radiance correlated moderately with Fe crystallinity (stronger crystallinity on slopes with higher radiance) and soil redness (redder soils on slopes with higher radiance). These patterns are typical manifestations of higher soil temperatures, longer dry periods, and lower vegetation density observed on predominately south-facing slopes (e.g., higher annual beam radiance) in the northern hemisphere (Reid, 1973; Birkeland, 1999; Rech et al., 2001). The positive correlation between slope angle and rock fragment content is in agreement with the process of colluviation (Table 2).

Slope angle had the largest correlation with soil properties within the metavolcanic terrain at SFREC, followed by CTI, annual beam radiance and mean curvature, and profile curvature (Table 2). Due to the larger sample size at SFREC, statistically significant ($p < 0.05$) Spearman correlation coefficients ranged from $\{0.19 \leq r_s \leq 1.0\}$. Despite the larger number of statistically significant correlations, the absolute value of the mean correlation between all pairs of aggregate soil properties and terrain attributes was 0.32, much lower than at SJER. Although correlation was low, two major pedogenic processes appeared to be captured by the correlation structure: (i) the aspect effect, influencing vegetation density, soil temperature, and soil moisture; and, (ii) terrain-induced re-distribution of soil moisture. Annual beam radiance was inversely correlated with thicker A horizons (greater organic inputs) and deeper soils (protection from erosion) on more shaded slopes (Table 2). Slope angle, CTI, and surface curvature were moderately correlated with soil properties that are typically affected by degree and duration of saturation. Convergent landscape positions (low slope angles and larger CTI) were correlated with higher CEC values, while divergent landscape positions (larger slope and smaller CTI) were correlated with stronger Fe crystallinity, Fe_d/Fe_{total}, and soil redness (Table 2). Contrary to these patterns, deeper soils and thicker Bt horizons (expected in convergent positions) were positively correlated with divergent positions. These two deviations from

Table 2. Spearman Rank Correlation coefficients (r_s) computed between select terrain and aggregate soil properties. The number of soil profiles used within each comparison is denoted in the "*n*" column. Coefficients are shown for correlations that were significant at the $p < 0.05$ level.

Site	Property	*n*	Annual beam radiance	Slope	Profile curvature	Mean curvature	CTI‡
SJER	A HZ† thickness, cm	15	–	–	–	–	–
	B HZ† thickness, cm	12	–	–	–	–	–
	Depth, cm	15	–	–	–	-0.74	0.66
	Rock fragments, %	15	–	0.53	–	–	–
	Redox features, %	15	–	–	–	-0.69	0.62
	Clay films, %	15	–	–	-0.54	–	–
	Clay, %	15	–	–	–	–	–
	CEC, cmol kg^{-1}	15	–	–	-0.74	-0.70	–
	Fe_d/Fe_{tot}	15	–	–	–	–	–
	Fe_d/Fe_o	15	-0.63	–	–	–	–
	Total C, %	15	–	–	–	–	–
	pH	15	–	–	–	-0.57	0.63
	Redness	15	0.55	–	–	0.56	-0.58
SFREC	A HZ† thickness, cm	106	-0.30	–	–	–	–
	B HZ† thickness, cm	106	–	0.35	0.29	0.19	-0.33
	Depth, cm	106	-0.27	0.29	–	–	-0.23
	Rock fragments, %	106	–	0.24	–	–	–
	Redox features, %	106	–	–	–	–	–
	Clay films, %	106	–	–	–	–	–
	Clay, %	65	–	–	–	–	–
	CEC, cmol kg^{-1}	45	–	-0.36	–	–	0.48
	Fe_d/Fe_{tot}	64	–	0.48	–	–	-0.25
	Fe_d/Fe_o	64	–	-0.30	–	–	0.27
	Total C, %	76	–	–	–	–	–
	pH	48	–	0.29	–	–	–
	Redness	74	–	0.64	–	0.29	-0.57

† Horizon.

‡ CTI-compound topographic index; Fe_d citrate–bicarbonate–dithionite extractable iron; Mn_d citrate–bicarbonate–dithionite manganese; Fe_o oxalate extractable iron; Mn_o oxalate extractable manganese; Fe_{tot} total iron measured by portable XRF.

the standard soil-landscape interpretation are likely related to the occurrence of deep soils with thick argillic horizons on topographic benches (convex profile curvature and moderate CTI) at SFREC. Perched water tables and lateral flow processes have been identified in the soils found on these landscape positions (Swarowsky et al., 2012). These unexpected patterns resemble the complex soil landscape relationships associated with old landscapes in the Rio Negro basin in southern Venezuela, where patches of well-developed, clay-rich soils were common in uplands and less developed sandy soils were found in low relief areas (Dubroeucq and Volkoff, 1998).

Evidence of Lithologic Variation

Spatial patterns in profile-weighted mean (total soil) Fe content were characterized by high spatial auto-correlation, spanning multiple landscape positions (Fig. 5). Total Fe measured on rock samples were generally in agreement (r= 0.81) with that of corresponding soil samples (Table 3). With the exception of rock samples "SJER-011" and "SFREC-n14", the ratio of soil-Fe to rock-Fe was within the range of 1.3 to 1.7.

Iron concentrations at SJER were correlated over distances up to approximately 100 m, and were generally within the expected levels of granite (2.14%), granodiorite (3.12%), and diorite (5.66%; Le Maitre, 1976). Dioritic patches were considerably smaller (~ 16% of the area) than the regions of granodiorite (~ 47% of the area), and granite (~37% of the area; Fig. 5). In contrast to observations by Pye (1986), terrain shape or rock outcrop abundance did not correspond to changes in lithology. Lithologic variability at SJER was predominately aligned with an apparent Ca–Fe gradient (PCA Axis 1) explaining 70% of total variance (Fig. 6). A secondary gradient primarily associated with total soil Zr, and largely orthogonal to Fe, explained an additional 22% of the variance (PCA Axis 2).

Total soil Fe concentrations at SFREC were correlated over larger distances as compared with SJER (up to approximately 650 m), and were generally close to the expected Fe content of basalt (8.30%; Le Maitre, 1976). Highest Fe concentrations (11–13%) were found in the upper portions of the catchment, especially along the eastern watershed boundary between sites "n29" and "n33" (Fig. 5). Variation in total soil Fe concentration was (spatially) associated with the two main drainages; however, this pattern was limited to middle elevations of the watershed. The largest variability in Fe concentration followed a SW–NE axis, and the lowest measured Fe value occurred on the knoll near soil profile "n09" (Fig. 5). The spatial patterns in rock composition at SFREC are likely related to the complex metamorphic setting of this region (Hacker, 1993). Lithologic variability at SFREC was predominately aligned with a gradient spanning low-Ca to high-Fe values (PCA Axis 1) explaining 65% of total variance (Fig. 6). A secondary, more complex, gradient associated with Ca and Zr concentrations (PCA Axis 2), explained an additional 22% of the variance.

Estimated Lithologic Influence on Soil Properties

Within each catena, there were strong correlations between horizon thickness-weighted mean soil properties and total soil Ca, Fe, and Zr. At SJER, variation in soil depth, abundance of clay films, clay content, CEC, and pH tracked weathering trajectories of granodiorite (less weatherable) and diorite (more weatherable; Table 4; Pye, 1986). However, Fe_d/Fe_{total} values and soil redness were negatively correlated with total soil Ca, and

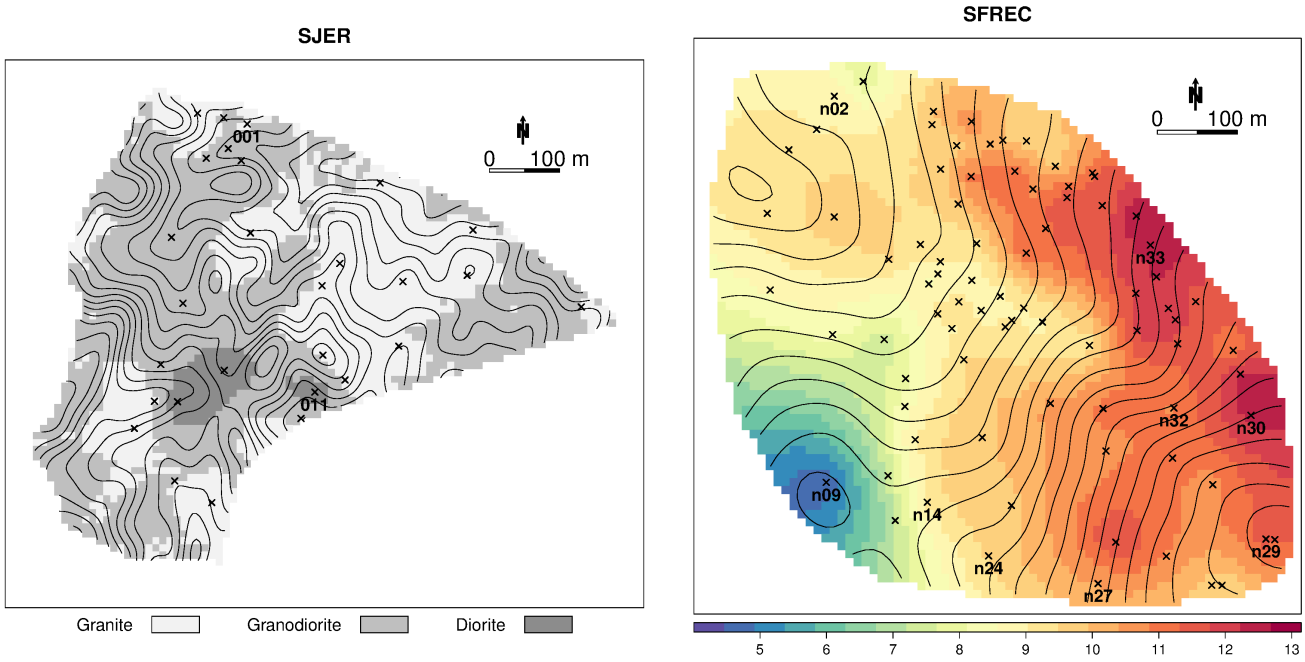

Fig. 5. Maps of lithologic variability at San Joaquin Experimental Range (SJER; CS, conditional simulation) and Sierra Foothill Research and Extension Center (SFREC; OK, ordinary kriging) based on horizon thickness-weighted mean, soil Fe concentrations (%) measured by XRF. Locations where elemental concentrations were measured on both rock and soil samples are labeled. Cross symbols correspond with locations where elemental concentrations were measured on soil samples, and solid lines correspond to elevation contours (2-m interval at SJER, 5-m interval at SFREC).

not significantly correlated with total soil Fe. These results are in conflict with the expected differences between soils formed on granodiorite vs. diorite, and may have been related to variation in soil age. Older, more stable summit positions may have had redder hues and greater iron oxide production, irrespective of total soil Fe content of the underlying rock. At SFREC, variation in Bt horizon thickness, soil depth, clay content, Fe_d/Fe_{total} values, and redness were correlated with total soil Fe, and to a lesser extent with total soil Zr (Table 4). Cation-exchange capacity was negatively correlated with total soil Fe, and positively correlated with total soil Ca suggesting that the formation of higher activity clays (e.g., smectite) was possibly favored in the presence of higher Ca concentration. Deeper soils, finer textures, and redder hues are commonly associated with soils formed from increasingly more mafic parent material (Graham and O'Geen, 2010).

Elemental concentrations measured on soil samples cannot always be interpreted as unbiased descriptors of lithologic variability. For example, Ca is mobile and actively biocycled once weathered from primary minerals; Fe and Zr can be enriched when other more mobile elements have been lost from or translocated within the soil profile (Birkeland, 1999; Fitzpatrick and Chittleborough, 2002). Manifestations of these processes are typically strongest in older, stable landscapes, and should result in a negative correlation between mobile elements and less mobile elements. At SJER, total soil Ca was positively correlated with total soil Fe, and at SFREC total soil Ca was nearly orthogonal (i.e., not correlated) to total soil Zr (Fig. 6). While these findings do not prove that these elements are unbiased descriptors of lithologic variability, it supports the interpretation that effective enrichment of Fe and Zr (relative to Ca) was not a major process within these catenas.

Interpretation of Soil-Landscape Correlations in the Presence of Lithologic Variability

Despite the large number of statistically significant correlations between terrain attributes and aggregate soil properties, causal relationships cannot be directly inferred when correlations with a third set of variables (elemental concentrations associated with parent material variability) are present (Legendre and Legendre, 1998). In other words, observed correlation between a given terrain attribute and soil property may be misleading when mutual correlation exists with an index of lithologic variability.

Table 3. Aggregate soil property and elemental concentration values from sites where elemental analysis was performed on rock samples. Clay content, pH, redness, citrate–bicarbonate–dithionite extractable iron (Fe_d) and total Fe (Fe_{tot}), are profile-weighted mean values.†

Sample	Soil depth	Clay	pH	Redness	Fe_d/Fe_{tot}	Fe_{tot}	Fe_{rock}	Fe_{tot}/Fe_{rock}
	cm	%				%	%	
SJER-01	85	8	6.0	8.3	0.11	2.3	1.8	1.3
SJER-11	130	16	6.2	9.0	0.10	6.1	6.8	0.9
SFREC-n02	80	20	5.6	10.0	0.33	9.3	7.4	1.3
SFREC-n09	57	14	5.8	8.8	0.32	4.2	2.5	1.7
SFREC-n14	84	27	5.7	12.9	0.35	9.6	3.1	3.1
SFREC-n24	170	30	5.6	10.8	0.36	9.63	7.44	1.3
SFREC-n27	71	31	5.9	15.2	0.44	10.3	6.1	1.7
SFREC-n29	120	34	5.9	15.1	0.48	11.9	8.9	1.4
SFREC-n30	134	51	6.2	14.5	0.65	12.6	8.8	1.4
SFREC-n32	80	26	6.0	15.4	0.42	10.7	6.3	1.7
SFREC-n33	135	41	6.4	15.5	0.55	12.4	8.8	1.4

† Fe_{tot} total iron measured by portable XRF; Fe_{rock} total Fe in rock samples measured by acid dissolution.

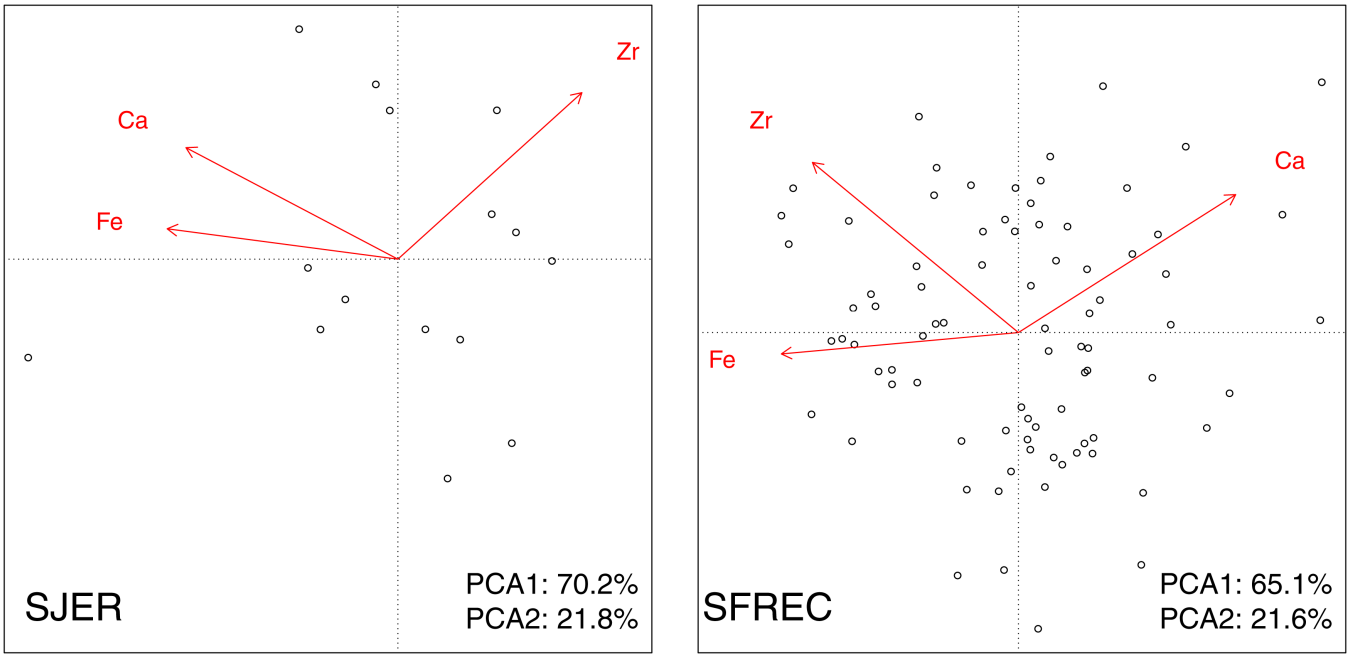

Fig. 6. Principle component analysis (PCA) biplots describing major axes of variation with respect to horizon thickness-weighted mean Ca, Fe, and Zr concentrations. Interpretation of the PCA biplot is analogous to interpretation of the RDA triplot (Supplemental Figure B).

Table 4. Spearman Rank Correlation coefficients (r_s) computed between select geochemical and aggregate soil properties. The number of soil profiles used within each comparison is denoted in the "*n*" column. Coefficients are only shown for correlations that were significant at the $p < 0.05$ level.

Site	Property	*n*	Ca	Fe	Zr
SJER	A HZ† thickness, cm	15	–	–	–
	B HZ† thickness, cm	12	–	–	–
	Depth, cm	15	0.53	0.66	-0.53
	Rock fragments, %	15	–	–	–
	Redox features, %	15	–	–	–
	Clay films, %	15	–	0.67	–
	Clay, %	15	–	0.74	–
	CEC, cmol kg^{-1}	15	–	0.87	–
	Fe_d/Fe_{tot}	15	-0.61	–	–
	Fe_d/Fe_o	15	–	–	–
	Total C, %	15	–	0.62	–
	pH	15	0.66	0.60	–
	Redness	15	-0.54	–	–
SFREC	A HZ† thickness, cm	106	-0.33	–	–
	B HZ† thickness, cm	106	-0.42	0.54	0.41
	Depth, cm	106	-0.35	0.48	0.36
	Rock fragments, %	106	-0.31	0.31	–
	Redox features, %	106	–	–	–
	Clay films, %	106	–	–	–
	Clay, %	65	-0.35	0.47	–
	CEC, cmol kg^{-1}	45	0.46	-0.61	-0.35
	Fe_d/Fe_{tot}	64	-0.54	0.78	0.56
	Fe_d/Fe_o	64	0.43	-0.73	-0.41
	Total C, %	76	–	0.27	–
	pH	48	–	–	–
	Redness	74	-0.43	0.78	0.55

† Horizon; Fe_d citrate–bicarbonate–dithionite extractable iron; Mn_d citrate–bicarbonate–dithionite manganese; Fe_o oxalate extractable iron; Mn_o oxalate extractable manganese; Fe_{tot} total iron measured by portable x-ray fluorescence.

At SJER, CEC was correlated with both convergent landscape positions ($r_s = -0.70$; Table 2) and higher total soil Fe ($r_s = 0.87$; Table 4), which was also strongly correlated with convergent landscape positions ($r_s = -0.73$; Table 5). Within the SFREC catena, Bt horizon thickness was correlated with steeper slopes ($r_s = 0.35$; Table 2) and higher total soil Fe ($r_s = 0.54$;Table 4), which was also positively correlated with steeper slope positions ($r_s = 0.44$; Table 5). In addition, total soil Ca was positively correlated with flatter and more convergent landscape positions, while total soil Fe and Zr followed the opposite pattern (Table 5). These findings complicate interpretation of soil–landscape relationships due to the presence of multiple, active soil-forming factors (relief and parent material), and the correlation between these factors.

Further investigation of the complex terrain-lithology correlation structure at each site was performed via RDA, using a subset of horizon thickness-weighted mean soil properties (Fig. 7). Redundancy analysis seeks to find a reduced set of new axes that describe variance in response variables: clay, CEC, redness (labeled as "A" in Fig. 7), pH, and Fe crystallinity (labeled as "feo_to_fed" in Fig. 7)—as constrained by explanatory variables: terrain shape indices (mean curvature, profile curvature, slope, annual beam radiance, and CTI) and indices of lithologic variability (total soil Ca, Fe, and Zr). These soil properties were selected because they reflect key sources of variability in soil classification and development within the SFR. Angular relationships between response (blue labels) and explanatory vectors (red arrows) are similar to correlations listed in Tables 2, 4, and 5. Correlation between explanatory variables, and their contribution to the RDA axes (RDA1 and RDA2 in Fig. 7) can be used to determine groups of explanatory variables that "share" information on variance in the response variables (soil proper-

ties). Within the SJER catena, RDA Axis 1 roughly corresponded to divergent vs. convergent landscape positions, and accounted for about 50% of the variance in select soil properties (Fig. 7). Total soil Ca contributed primarily to RDA Axis 1 and was highly correlated with convergent landscape positions, which complicates its utility as an index of lithologic variability (Fig. 7). The correlation between total soil Ca and indices of terrain shape at SJER is not surprising given the high potential rate of leaching due to coarse soil textures (loamy coarse sands and coarse sandy loams). Downslope movement of Ca weathered from primary minerals (anorthite and hornblende) result in net loss of Ca from divergent positions and net gain of Ca in convergent positions where cation exchange and neoformation retain Ca. Redundancy analysis Axis 2 at SJER roughly corresponds to the gradation in parent material from predominately dioritic sources (low total soil Zr, high total soil Fe) to predominately granodioritic/granitic sources (lower total soil Fe, high total soil Zr), and accounts for 26% of the variance in soil properties (Fig. 7). However, total soil Fe and Zr also contribute to RDA Axis 1, suggesting that these variables share information with terrain shape indices. Modeled annual beam radiance contributes nearly equally to RDA Axes 1 and 2, and is more or less orthogonal to total soil Ca, Fe and Zr. Additional details on the interpretation of RDA triplots are given in Supplemental Figure B. A more detailed description of the theory behind RDA from a soil survey perspective is given in Odeh et al. (1991).

In contrast with SJER, there was considerable overlap in information shared by terrain shape indices and elemental concentration within the SFREC catena (Fig. 7). Redundancy analysis Axis 1 at SFREC described 37% of the variance in soil properties, and was aligned with a gradient in total soil Fe. Slope angle, profile curvature, mean curvature, CTI, and total soil Zr all contributed to RDA Axis 1. Total soil Ca and Zr, along with annual beam radiance all contributed to RDA Axis 2, which described 5% of the variance in soil properties (Fig. 7). It is clear that considerable information is shared between terrain shape indices and elemental concentrations within this catena—severely impairing any causal interpretation of terrain-induced variation in soil properties.

Table 5. Spearman Rank Correlation coefficients (r_s) computed between select terrain and profile-weighted mean Ca, Fe, and Zr concentrations. The number of soil profiles used within each comparison is denoted in the "*n*" column. Coefficients are only shown for correlations that were significant at the $p < 0.05$ level.

Site	Element	*n*	Annual beam radiance	Slope	Profile curvature	Mean curvature	CTI†
SJER	Ca	15	–	–	–	-0.54	0.70
	Fe	15	–	–	-0.81	-0.73	0.54
	Zr	15	–	–	–	–	–
SFREC	Ca	64	–	-0.47	–	-0.28	0.37
	Fe	64	–	0.44	0.37	0.39	-0.47
	Zr	64	0.23	0.24	–	–	–

† CTI-compound topographic index.

Whole-Profile Variance Partitioning

Partial RDA was used to determine the approximate amount of partial variance in soil properties (clay content, redness, CEC, pH, and Fe crystallinity) explained by the terrain shape indices, lithologic indices, and depth (RCS basis functions). The amount of variance accounted for by the combination of terrain, litho-

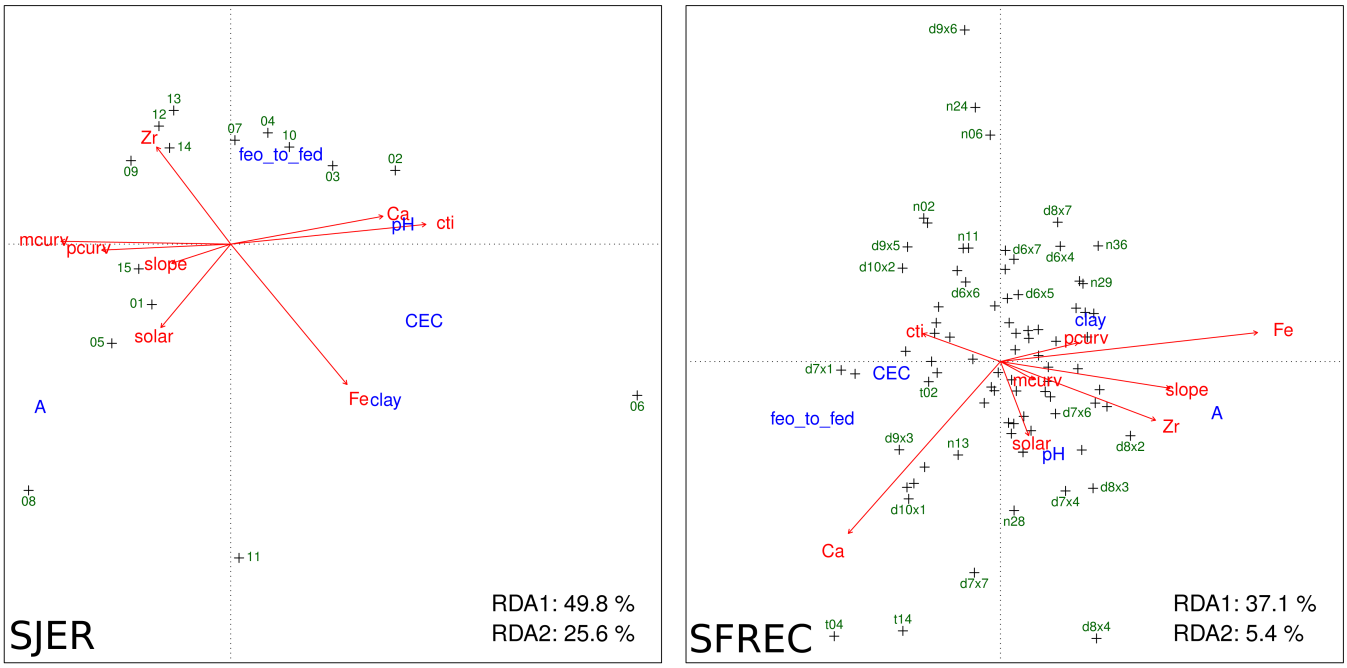

Fig. 7. Redundancy analysis (RDA) triplots of horizon thickness-weighted mean soil properties (blue labels) vs. soil elemental concentrations and terrain shape indices (red labels). Redundancy analysis Axis 1 corresponds to the x axis, and RDA Axis 2 corresponds to the y axis. Site identifications are included for the 15 soils sampled at San Joaquin Experimental Range (SJER), and select soils sampled at Sierra Foothill Research and Extension Center (SFREC). Interpretation of the RDA triplot is described in Supplemental Figure B.

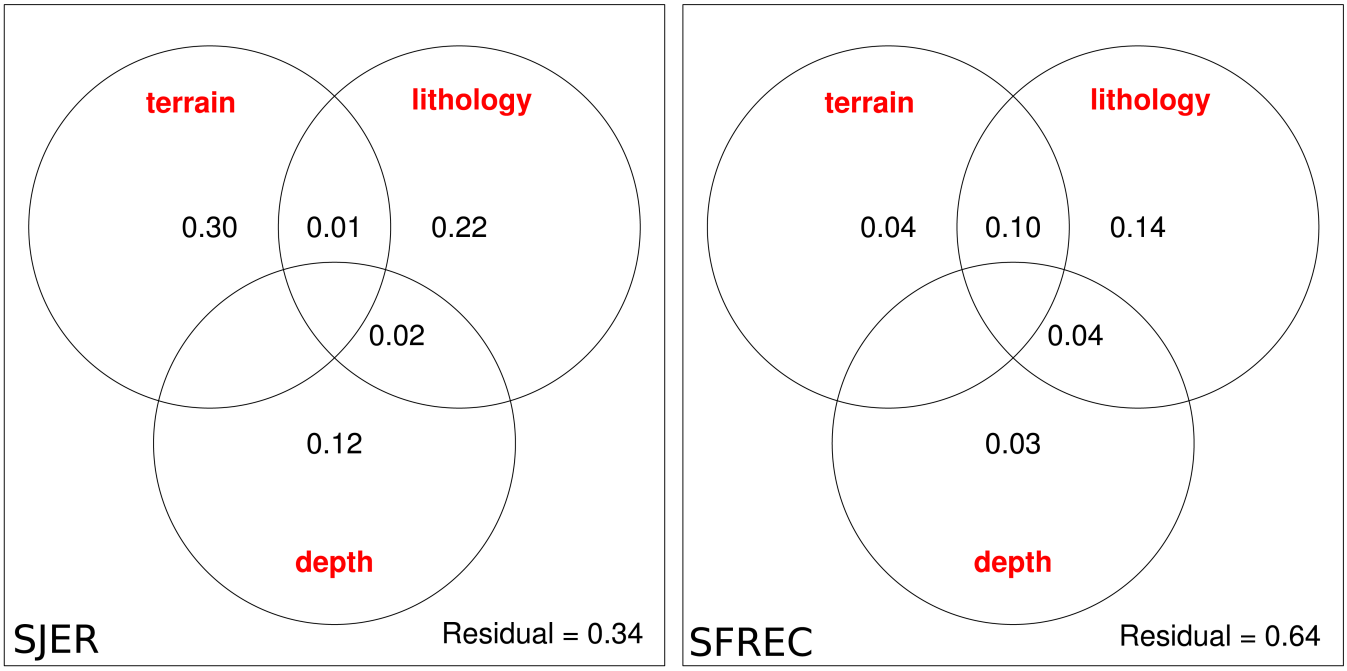

Fig. 8. Variance partitioning performed via pRDA, on 10-cm depth slices. Variance in clay content, redness, cation-exchange capacity (CEC), pH, and Fe crystallinity was partitioned across terrain shape indices, lithologic indices, and restricted cubic splines (RCS) basis functions. Values < 0.01 omitted.

logic, and depth variable suites varied from 66% (SJER) to 36% (SFREC; Fig. 8). Terrain variables alone accounted for 30% of the variance in soil properties at SJER, but only 4% at SFREC. This finding follows field-based observations: the classically defined hillslope sequences (e.g., summit → shoulder → backslope → footslope → swale, etc.) at SJER gives rise to consistent relationships between terrain shape and soil properties (Ruhe, 1956). While at SFREC the presence of highly weathered soils on complex, non-repeating hillslope sequences (e.g., summit → backslope → bench → incised channel → knoll → shoulder, etc.) results in less systematic soil-landscape relationships. Due to the larger characteristic size of landforms at SFREC (400–700 m from summit to corresponding footslope) as compared with SJER (80–120 m from summit to corresponding footslope), replicated sampling within classically defined landscape positions was limited at SFREC. A future study involving an expanded study area in the metamorphic belt of the SFR could result in better estimates of how variance in soil properties is partitioned between terrain and lithology.

Elemental variables, used to describe lithologic variability, accounted for 22% of the variance in soil properties at SJER, and 14% at SFREC. Lithologic variability at SJER was largely related to the presence of diorite inclusions within a granite-granodiorite matrix. At SFREC lithologic variability was mostly associated with variable Ca and Fe content of the bedrock (meta-basalt grading into meta-andesite).

Depth basis functions accounted for 12% of the variance in "soil character" at SJER, but only 3% at SFREC (Fig. 8). Overlapping regions of Fig. 8 represent proportions of variance in response variables accounted for by the combination of two or more suites of predictor variables. The 10% of variance in soil properties (SFREC) explained by the combination of terrain and lithologic variables further suggests concurrent soil-forming factors: (i) a parent material influence on weathering trajectories within the profile; and, (ii) a topographic influence on the redistribution of sediment and weathering products throughout the catena.

Application of Redundancy Analysis and Other Ordination Methods in Soil Survey

There are few cases where soil formation has not been affected by several (likely concurrent) soil forming processes. Redundancy analysis and related ordination methods provide a useful framework for initial investigation of complex soil-landscape relationships (Odeh et al., 1991). In particular, RDA and pRDA can help determine the relative importance of superposed soil-forming processes or ecological gradients (Peres-Neto et al., 2006). Once an optimal subset of pedologically plausible covariates have been identified (via RDA), other methods such as regression or classification are typically more successful at generating predictions for single soil properties or classes (Legendre and Legendre, 1998). Identification of regionally important sets of covariates is perhaps one of the most important requirements to successful downscaling (or disaggregation) of existing soil survey data (Nauman and Thompson, 2014; Subburayalu et al., 2014).

Options for Detailed Mapping of Lithologic Variability

Within the large body of literature on the topic of "digital soil mapping", parent material co-variates are not frequently incorporated (relative to terrain shape co-variates or other soil properties) into predictive models of soil variation (McBratney et al., 2003;

Scull et al., 2003; Grunwald, 2009). The use of field-portable XRF devices offer an exiting, albeit expensive, approach to rapidly identifying and quantifying local variation in lithology (Zhu et al., 2011; Weindorf et al., 2012; McLaren et al., 2012). In arid environments, multispectral (Landsat TM), and hyperspectral (AVIRIS) remote sensing has been used to delineate variation in surface mineralogy and sediment source (Scull et al., 2003; Levi and Rasmussen, 2014). However, band ratios and spectral signatures used to differentiate mineral assemblages are not likely to generalize well to temperate or humid regions unless patterns in vegetation density and species composition consistently track patterns in lithology. Aside from traditional geologic maps, the only widely used (but not necessarily widely available) proxy for lithologic variability is γ-ray spectroscopy (Cook et al., 1996; McKenzie and Ryan, 1999; Wilford, 2012). The combination of airborne γ-ray and magnetic anomaly (McCafferty and Gosen, 2009) measurements may support rapid assessment of key lithologic variables at spatial scales relevant to soil-landscape modeling.

CONCLUSIONS

The potential for using DEM-derived indices of terrain shape to predict spatial patterns in soil properties varied greatly between our two experimental catenas. A QSM approach is best suited for granitic landscapes of the SFR where the degree of soil development is closely linked with topographic focusing of water. Our findings suggest that to be effective, any quantitative soil mapping effort must account for multiple superposed soil-forming processes that likely vary in both space and time. This study supports the widely stated shortcoming of QSM that better digital proxies are needed to describe the effects of organisms, time, and parent material on soil development.

ACKNOWLEDGMENTS

We thank Alexandre Swarowsky and Tony Orozco for assistance with soil description and sampling SFREC and SJER catenas. We also thank Jaiyou Deng for his contributions to laboratory work supporting this study, and the staff at SJER and SFREC for their support. We would like to thank Dr. Laura Stupi (Thermo Fischer Scientific) for lending us two portable XRF devices over the summer of 2010. This work was funded by the Kearney Foundation of Soil Science and in part by the National Science Foundation, award #1331939.

REFERENCES

Beaudette, D.E., R.A. Dahlgren, and A.T. O'Geen. 2013a. Terrain shape indices for modelling soil moisture dynamics. Soil Sci. Soc. Am. J. 77:1696–1710. doi:10.2136/sssaj2013.02.0048

Beaudette, D.E., P. Roudier, and A.T. O'Geen. 2013b. Algorithms for quantitative pedology: A toolkit for soil scientists. Comput. Geosci. 52:258–268.

Birkeland, P.W. 1999. Soils and geomorphology. 3rd ed. Oxford Univ. Press, New York.

Bishop, T.F.A., A.B. McBratney, and G.M. Laslett. 1999. Modelling soil attribute depth functions with equal-area quadratic smoothing splines. Geoderma 91:27– 45.

Brown, D.J., M.K. Clayton, and K. McSweeney. 2004. Potential terrain controls on soil color, texture contrast and grain-size deposition for the original catena landscape in Uganda. Geoderma 122:51–72.

Carre, F., and A.B. McBratney. 2005. Digital terron mapping. Geoderma 128:340–353. doi:10.1016/j.geoderma.2005.04.012

Cook, S., R. Corner, P. Groves, and G. Grealish. 1996. Use of airborne gamma radiometric data for soil sampling. Aust. J. Soil Res. 34:183–194. doi:10.1071/SR9960183

de Gruijter, J., D. Brus, M. Bierkens, and M. Knotters. 2006. Sampling for natural resource monitoring. Springer, New York.

Dubroeucq, D., and B. Volkoff. 1998. From Oxisols to Spodosols and Histosols: Evolution of the soil mantles in the Rio Negro basin (Amazonia). Catena 32:245–280. doi:10.1016/S0341-8162(98)00045-9

Fitzpatrick, R., and D. Chittleborough. 2002. Titanium and zirconium minerals. In: J. Dixon and D. Schulze, editors, Soil mineraology with environmental applications. SSSA, Madison, WI. p. 667–690.

Gee, G., and D. Orr. 2002. Particle-size analysis. In: J. Dane and G. Topp, editors, Methods of soil analysis: Physical methods. SSSA Book Ser. No. 5, SSSA, Madison, WI. p. 255–293.

Gessler, P., O. Chadwick, F. Charman, L. Althouse, and K. Holmes. 2000. Modeling soil-landscape and ecosystem properties using terrain attributes. Soil Sci. Soc. Am. J. 64:2046–2056. doi:10.2136/sssaj2000.6462046x

Goovaerts, P. 1999. Geostatistics in soil science: State-of-the-art and perspectives. Geoderma 89:1–45. doi:10.1016/S0016-7061(98)00078-0

Graham, R., and A. O'Geen. 2010. Soil mineralogy trends in California landscapes. Geoderma 154:418–437. doi:10.1016/j.geoderma.2009.05.018

GRASS Development Team. 2009. Geographic resources analysis support system (GRASS GIS) Software. ITC-irst, Trento, Italy.

Grunwald, S. 2009. Multi-criteria characterization of recent digital soil mapping and modeling approaches. Geoderma 152:195–207. doi:10.1016/j.geoderma.2009.06.003

Hacker, B.R. 1993. Evolution of the northern Sierra Nevada metamorphic belt: Petrological, structural, and Ar/Ar constraints. Geol. Soc. Am. Bull. 105:637–656. doi:10.1130/0016-7606(1993)105<0637:EOTNSN>2.3.CO;2

Harrell, F.E. 2001. Regression modeling strategies. Springer Series in Statistics. Springer, New York.

Hastie, T., R. Tibshirani, and J. Friedman. 2009. The elements of statistical learning. Springer, New York.

Hengl, T., G.B. Heuvelink, and A. Stein. 2004. A generic framework for spatial prediction of soil variables based on regression-kriging. Geoderma 120:75–93. doi:10.1016/j.geoderma.2003.08.018

Hengl, T., and D. Rossiter. 2003. Supervised landform classification to enhance and replace photo-interpretation in semi-detailed soil survey. Soil Sci. Soc. Am. J. 67:1810–1822. doi:10.2136/sssaj2003.1810

Hudson, B.D. 1992. The soil survey as paradigm-based science. Soil Sci. Soc. Am. J. 56:836–841. doi:10.2136/sssaj1992.03615995005600030027x

Indorante, S.J., J.M. Kabrick, B.D. Lee, and J.M. Maatta. 2014. Quantifying soil profile change caused by land use in central Missouri loess hillslopes. Soil Sci. Soc. Am. J. 78:225–237. doi:10.2136/sssaj2013.07.0285

Issaks, E.H., and R.M. Srivastava. 1989. An introduction to applied geostatistics. Oxford Univ. Press, Oxford.

Jenny, H. 1941. Factors of soil formation: A system of quantitative pedology. McGraw-Hill, New York.

King, G.J., D.F. Acton, and R.J. St. Arnaud. 1983. Soil-landscape analysis in relation to soil distribution and mapping at a site within the Weyburn association. Can. J. Soil Sci. 63:657–670. doi:10.4141/cjss83-067

Liles, G.C., D.E. Beaudette, A.T. O'Geen, and W.R. Horwath. 2013. Developing predictive soil C models for soils using quantitative color measurements. Soil Sci. Soc. Am. J. 77:2173–2181. doi:10.2136/sssaj2013.02.0057

Le Maitre, R. 1976. The chemical variability of some common igneous rocks. J. Petrol. 17:589–637. doi:10.1093/petrology/17.4.589

Legendre, P., and L. Legendre. 1998. Numerical ecology In: Developments in environmental modeling. 2nd ed. No. 20. Elsevier, Amsterdam.

Levi, M.R., and C. Rasmussen. 2014. Covariate selection with iterative principal component analysis for predicting physical soil properties. Geoderma 219-220:46–57. doi:10.1016/j.geoderma.2013.12.013

Llobera, M. 2001. Building past landscape perception with GIS: Understanding topographic prominence. J. Archaeol. Sci. 28:1005–1014. doi:10.1006/jasc.2001.0720

Malone, B., A. McBratney, B. Minasny, and G. Laslett. 2009. Mapping continuous depth functions of soil carbon storage and available water capacity. Geoderma 154:138–152. doi:10.1016/j.geoderma.2009.10.007

McBratney, A.B., T.F.A. Bishop, and I.S. Teliatnikov. 2000. Two soil profile reconstruction techniques. Geoderma 97:209– 221.

McBratney, A.B., M.L. Mendonca Santos, and B. Minasny. 2003. On digital soil mapping. Geoderma 117:3–52. doi:10.1016/S0016-7061(03)00223-4

McCafferty, A., and B.V. Gosen. 2009. Airborne gamma-ray and magnetic anomaly signatures of serpentinite in relation to soil geochemistry, northern California. Appl. Geochem. 24:1524–1537. doi:10.1016/j.apgeochem.2009.04.007

McKeague, J., and J. Day. 1966. Dithionite and oxalate extractable fe and al as aids in differentiating various classes of soils. Can. J. Soil Sci. 46:13–22. doi:10.4141/cjss66-003

McKenzie, N.J., and P.J. Ryan. 1999. Spatial prediction of soil properties using environmental correlation. Geoderma 89:67–94. doi:10.1016/S0016-7061(98)00137-2

McLaren, T.I., C.N. Guppy, M.K. Tighe, N. Forster, P. Grave, L.M. Lisle, and J.W. Bennett. 2012. Rapid, nondestructive total elemental analysis of vertisol soils using portable x-ray fluorescence. Soil Sci. Soc. Am. J. 76:1436–1445. doi:10.2136/sssaj2011.0354

Minasny, B., and A.B. McBratney. 2007. Incorporating taxonomic distance into spatial prediction and digital mapping of soil classes. Geoderma 142:285–293. doi:10.1016/j.geoderma.2007.08.022

Mitasova, H., and J. Hofierka. 1993. Interpolation by regularized spline with tension: II. Application to terrain modeling and surface geometry analysis. Math. Geol. 25:657–669. doi:10.1007/BF00893172

Mitasova, H., and L. Mitas. 1993. Interpolation by regularized spline with tension: I. Theory and implementation. Math. Geol. 25:641–655. doi:10.1007/BF00893171

Mishra, U., R. Lal, B. Slater, F. Calhoun, D. Liu, and M.V. Meirvenne. 2009. Predicting soil organic carbon stock using profile depth distribution functions and ordinary kriging. Soil Sci. Soc. Am. J. 73:614–621. doi:10.2136/sssaj2007.0410

Moore, I., R. Grayson, and A. Ladson. 1991. Digital terrain modelling: A review of hydrological, geomorphological, and biological applications. Hydrol. Processes 5:3–30. doi:10.1002/hyp.3360050103

Myers, D.B., N.R. Kitchen, K.A. Sudduth, R.J. Miles, E.J. Sadler, and S. Grunwald. 2011. Peak functions for modeling high resolution soil profile data. Geoderma 166:74–83. doi:10.1016/j.geoderma.2011.07.014

Nauman, T.W., and J.A. Thompson. 2014. Semi-automated disaggregation of conventional soil maps using knowledge driven data mining and classification trees. Geoderma 213:385–399. doi:10.1016/j.geoderma.2013.08.024

Odeh, I., D. Chittleborough, and A. McBratney. 1991. Elucidation of soil-landform interrelationships by canonical ordination analysis. Geoderma 49:1–32.

Oksanen, J.F., G. Blanchet, R. Kindt, P. Legendre, P. R. Minchin, R. B. O'Hara, G. L. Simpson, P. Solymos, M. Henry, H. Stevens, and H. Wagner, 2015. Vegan: Community ecology package. R package version 2.2-1.

Park, S., K. McSweeney, and B. Lowery. 2001. Identification of the spatial distribution of soils using a process-based terrain characterization. Geoderma 103:249–272. doi:10.1016/S0016-7061(01)00042-8

Peres-Neto, P.R., P. Legendre, S. Dray, and D. Borcard. 2006. Variation partitioning of species data matrices: Estimation and comparison of fractions. Ecology 87:2614–2625. doi:10.1890/0012-9658(2006)87[2614:VPOSDM]2.0.CO;2

Pye, K. 1986. Mineralogical and textural controls on the weathering of granitoid rocks. Catena 13:47–57. doi:10.1016/S0341-8162(86)80004-2

R Core Team. 2014. R: A language and environment for statistical computing. R Foundation for Statistical Computing, Vienna, Austria. Available at http://www.R-project.org/ (verified 23 Feb. 2016).

Rech, J.R., R.W. Reeves, and D.M. Hendricks. 2001. The influence of slope aspect on soil weathering processes in the Springerville volcanic fieild, Arizona. Catena 43:49–62. doi:10.1016/S0341-8162(00)00118-1

Reid, I. 1973. The influence of slope orientation upon the soil moisture regime, and its hydrogeomorphological significance. J. Hydrol. 19:309–321. doi:10.1016/0022-1694(73)90105-4

Rigollier, C., O. Bauer, and L. Wald. 2000. On the clear sky model of the ESRA–European Solar Radiation Atlas–with respect to the Heliosat method. Sol. Energy 68:33–48. doi:10.1016/S0038-092X(99)00055-9

Ruhe, R.V. 1956. Geomorphic surfaces and the nature of soils. Soil Sci. 82:441–455. doi:10.1097/00010694-195612000-00001

Scull, P., J. Franklin, O. Chadwick, and D. McArthur. 2003. Predictive soil mapping: A review. Prog. Phys. Geogr. 27:171–197. doi:10.1191/0309133303pp366ra

Soil Survey Staff. 1999. Soil taxonomy: A basic system of soil classification for making and interpreting soil surveys. 2nd ed. Natural Resources Conservation Service. U.S. Department of Agriculture Handb. 436.U.S. Gov. Print. Office, Washington, DC.

Soil Survey Staff. 2004. Soil survey laboratory methods manual. 4th ed. No. 42 In Soil Survey Investigations Report. USDA-NRCS, Washington, DC.

Soil Survey Staff. 2012. Field book for describing and sampling soils, Ver. 3.0. Natural Resources Conservation Service. U.S. Department of Agriculture, Washington, DC.

Subburayalu, S.K., I. Jenhani, and B.K. Slater. 2014. Disaggregation of component soil series on an Ohio County soil survey map using possibilistic decision trees. Geoderma 213:334–345. doi:10.1016/j.geoderma.2013.08.018

Swarowsky, A., R.A. Dahlgren, and A.T. O'Geen. 2012. Linking subsurface lateral flowpath activity with streamflow characteristics in a semiarid headwater catchment. Soil Sci. Soc. Am. J. 76:532–547. doi:10.2136/sssaj2011.0061

Thompson, J.A., E.M. Pena-Yetukhiw, and J.H. Grove. 2006. Soil-landscape modeling across a physiographic region: Topographic patterns and model transportability. Geoderma 133:57–70. doi:10.1016/j.geoderma.2006.03.037

Verheyen, K., D. Adriaens, M. Hermy, and S. Deckers. 2001. High-resolution continuous soil classification using morphological soil profile descriptions. Geoderma 101:31–48. doi:10.1016/S0016-7061(00)00088-4

Verzani, J. 2004. Using R for Introductory Statistics. Chapman & Hall, London.

Viscarra Rossel, R.A., B. Minasny, P. Roudier, and A.B. McBratney. 2006. Colour space models for soil science. Geoderma 133:320–337. doi:10.1016/j.geoderma.2005.07.017

Weindorf, D. C., Y. Zhu, B. Haggard, J. Lofton, S. Chakraborty, N. Bakr, W. Zhang, W. C. Weindorf, and M. Legoria, 2012. Enhanced pedon horizonation using portable x-ray fluorescence spectrometry. Soil Sci. Soc. Am. J. 76:522–531. doi:10.2136/sssaj2011.0174

Wilford, J.A. 2012. A weathering intensity index for the Australian continent using airborne gamma-ray spectrometry and digital terrain analysis. Geoderma 183–184:124–142. doi:10.1016/j.geoderma.2010.12.022

Wilson, J.P., and J.C. Gallant. 2000. Secondary terrain attributes. In: J.P. Wilson and J.C. Gallant, editors, Terrain Analysis: Principles and Applications. John Wiley & Sons, New York. p. 87–131.

Young, F., and R. Hammer. 2000. Defining geographic soil bodies by landscape position, soil taxonomy, and cluster analysis. Soil Sci. Soc. Am. J. 64:989–998. doi:10.2136/sssaj2000.643989x

Zhu, Y., D.C. Weindorf, and W. Zhang. 2011. Characterizing soils using a portable x-ray fluorescence spectrometer: 1. soil texture. Geoderma 167:168:167– 177.